6-28-2014

Role of strain on electronic and mechanical response of semiconducting transition-metal dichalcogenide monolayers: An ab-initio study

David M. Guzman
Purdue University, guzmand@purdue.edu

Alejandro Strachan
Purdue University, Birck Nanotechnolgy Center, strachan@purdue.edu

David M. Guzman and Alejandro Strachan

Role of strain on electronic and mechanical response of semiconducting transition-metal dichalcogenide monolayers: An *ab-initio* study

David M. Guzman and Alejandro Strachan[a)]

School of Materials Engineering and Birck Nanotechnology Center, Purdue University, West Lafayette, Indiana 47907-2044, USA

We characterize the electronic structure and elasticity of monolayer transition-metal dichalcogenides MX_2 (M = Mo, W, Sn, Hf and X = S, Se, Te) based on 2H and 1T structures using fully relativistic first principles calculations based on density functional theory. We focus on the role of strain on the band structure and band alignment across the series of materials. We find that strain has a significant effect on the band gap; a biaxial strain of 1% decreases the band gap in the 2H structures, by as a much as 0.2 eV in MoS_2 and WS_2, while increasing it for the 1T cases. These results indicate that strain is a powerful avenue to modulate their properties; for example, strain enables the formation of, otherwise impossible, broken gap heterostructures within the 2H class. These calculations provide insight and quantitative information for the rational development of heterostructures based on this class of materials accounting for the effect of strain. © *2014 AIP Publishing LLC*. [http://dx.doi.org/10.1063/1.4883995]

I. INTRODUCTION

Since the successful exfoliation of one-atom-thick materials[1] interest in two-dimensional (2D) structures has grown hand in hand with our ability to control their synthesis,[2,3] the characterization of their unique properties[4,5] and their initial use in devices.[6–8] Many of the unique physical properties of this new class of materials result from quantum confinement and control of the number of layers can be used to tune their properties. Strain also has a strong effect on their electronic properties and whether engineered or unwanted it affects applications.[9] The significant efforts in basic and applied science around graphene have been accompanied by growing interest in developing a menu of 2D materials that would offer the variety in electronic properties (e.g., band gaps, band offsets, and carrier mobilities) needed for device applications. For example, type-II heterostructures would be interesting for photovoltaics and type-III heterostructures for mid-wave infrared light sources and band-to-band tunnel field effect transistors. Progress in the development and characterization of 2D materials and associated devices would benefit significantly from theoretical guidance in the form of property predictions for known and possible structures.

Bulk transition-metal dichalcogenides (MX_2) are an attractive starting point for 2D materials design due to their layered structures and wide variety of physical properties, ranging from semiconductors, as in the case of (Mo, W)X_2, to superconductors like NbS_2. High yield and reproducibility of MX_2 single-layer nanosheets can be achieved from the bulk through lithium intercalation in an electrochemical set up,[10] which is attractive for their application in the electronics industry. Some transition-metal dichalcogenides have been successfully produced as single layers[1,11–14] and the electronic structure of single- and few-layer Mo and W dichalcogenides has been extensively investigated

experimentally.[15–20] Complementing the experimental work, *ab initio* techniques have been used to predict the properties of a wider range of possible 2D dichalcogenides.[21,22] Simulations have been used to assess the effect of the number of monolayers on electronic structure[17,23] and to predict band alignments across a large number of materials. From an application point of view, MX_2 monolayers are being integrated into devices. Examples include MoS_2 monolayer based transistors[24] and integrated circuits to perform logic operations.[25] Other applications for photovoltaic devices,[26,27] vapor sensing,[28] spontaneous water photo-splitting,[14,29] and spintronics[30] have also been proposed and studied.

Strain represents both a significant challenge but also an opportunity as MX_2 monolayers are integrated into devices. Integration of 2D materials almost invariably leads to mechanical strain due to the lattice parameter or thermal expansion coefficient mismatch. Consequently, the role of strain on band structure and alignment and the materials stiffness are critical pieces of information needed for rational device design. Recent reports quantified the effect of mechanical strain on the electronic structure[23,31] and the band offsets[29,32] of some MX_2 single-layer systems. In this paper, we characterize the role of biaxial strain on the band structure and alignment of a series of MX_2 monolayers consisting of M = Mo, W, Sn, Hf and X = S, Se, and Te using density functional theory (DFT). The results confirm the possibility of creating type-II and type-III heterostructures and provide insight into the levels of strain admissible to achieve them.

II. METHODOLOGY

A. Atomic structure of dichalcogenides

Bulk Mo and W dichalcogenides crystallize in a 4H structure with space group $P6_3/mmc$ (194) that consists of X-M-X slabs weakly bonded though van der Waals interactions. The space group symmetry is reduced to P-6m2 (187) in the single-layer system due to the loss of inversion

---

a)Author to whom correspondence should be addressed. Electronic mail: strachan@purdue.edu

symmetry; the structure, shown Figure 1(a), is known as 2H, see Figure 1(a). Bulk Sn and Hf dichalcogenides adopt the so-called 1T structure with space group P-3m1 (164) identical to cadmium iodide (CdI_2); again, the individual layers are held together through weakly by van der Walls forces. A single layer of this structure is shown in Figure 1(b). The MX_2 layers consist of metal atoms sandwiched between chalcogens through ionic-covalent bond forming a trigonal prismatic coordination for M = Mo and W, Figure 1(a), and a distorted octahedral coordination for M = Sn and Hf, Figure 1(b).

B. Simulation details

All calculations were carried out using the all-electron, full-potential, linear augmented plane wave (FP-LAPW) method as implemented in the WIEN2k code.[33] The exchange-correlation potential was calculated using the generalized gradient approximation as proposed by Perdew, Burke, and Ernzerhof (PBE).[34] The muffin-tin radii for the chalcogen atoms was taken as RMT = 2.1 a.u., while for the Mo and W atoms RMT = 2.3 a.u., and for the Sn and Hf atoms RMT = 2.5 a.u. We set the cutoff wave vector K_{max} parameter to $RMT*K_{max}$ = 7. The valence electrons wave functions inside the muffin-tin spheres are expanded in terms of spherical harmonics up to l_{max} = 10, and in terms of plane waves with a wave vector cutoff K_{max} in the interstitial region.

The two-dimensional structures are modeled as periodic slabs with a sufficiently large c-lattice constant (25 Å) to avoid interactions between adjacent layers. The in-plane lattice constant a and the internal position parameter z are optimized with a strict force convergence of 1 mRy/Bohr. The electronic integration is taken over a commensurate k-mesh of 105×105 in the two-dimensional Brillouin zone, shown in Figure 1(c) and the convergence of the self-consistent field calculations is attained with a tolerance in total energy of

0.01 mRy. Spin-orbit interaction is included in the Hamiltonian through the second variational method[35] and is taken into account in the band structure. The vacuum level is taken as zero energy when calculating the band alignment. We note that throughout this paper, the band structures reported are obtained from the Kohn-Sham eigenvalues in the DFT calculations; while this is standard, it is known to underestimate the band gap in semiconductors as discussed in Sec. II C.

C. GW correction of bandstructures

Fully converged GW calculations of the band-edge energies of molybdenum and tungsten chalcogenides[32] indicate that the absolute valence band (VB) maximum and conduction band (CB) minimum energies can be accurately described using the band-gap-center (BGC) approximation, as proposed by *Toroker et al.*[36] In this approximation, the band-gap-center energy (E_{BGC}) is determined from the DFT-PBE calculation as the average between the VB maximum and CB minimum energies. The absolute position of the band edges is then corrected with the quasiparticle gap energy (E_{QP}) assuming a symmetric band gap opening with respect to the BGC energy; that is:

$$E_{CBM} = E_{BGC} + \frac{1}{2} E_{QP},$$

$$E_{VBM} = E_{BGC} - \frac{1}{2} E_{QP}.$$

As noted in Ref. 32, the BGC approximation is useful to estimate the absolute band-edge positions of this class of 2D materials without performing the costly fully converged GW calculation, as only the quasiparticle band gap energy is necessary. Furthermore, the GW corrected energy gaps reported by Liang *et al.* suggest a band gap opening of approximately 50% with respect to the DFT-PBE prediction. Thus, in discussing the implications of our work, we will consider the 50% correction to the DFT-PBE calculated band-edge energies, assuming a symmetric band-gap opening with respect to E_{BGC}, as was done in Ref. 22. None of the figures include the GW correction.

D. Elastic constants

The elastic properties calculations of MX_2 monolayer systems are performed with the Quantum Espresso[37] package using the PBE[34] implementation of GGA for the exchange-correlation potential and projector-augmented wave[38] (PAW) pseudopotentials for the core electrons. All the simulations used a plane-wave basis set with kinetic energy of 40 Ry and a Brillouin zone sampling of $10\times10\times1$ k points within the Monkhorst-Pack method.[39] The atomic structure of the MX_2 monolayers was represented with a 2×1 rectangular periodic supercell with respect to the hexagonal unit cell. In order to suppress the interaction between adjacent slaps, a vacuum layer of 25 Å was added in the c-axis. The structural optimization is carried out using the BFGS quasi-Newton method with energy and force convergence criteria of 10^{-6} Ry and 1 mRy/Bohr, respectively.
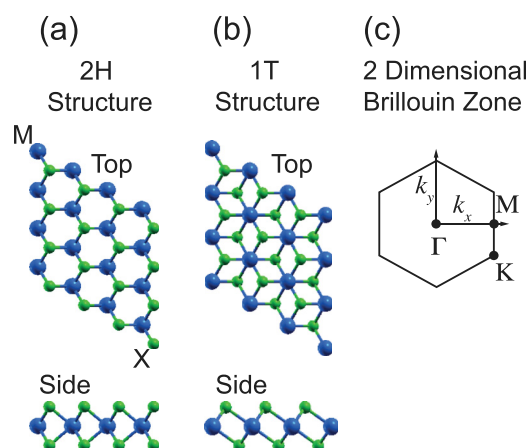

FIG. 1. (a) Top and side view of 2H MX_2 monolayers (M = Mo, W and X = S, Se) crystal structure with space group symmetry P-6m2. (b) Top and side view of 1T MX_2 monolayers (M = Sn, Hf and X = S, Se) crystal structure with space group symmetry P-3m1. (c) Two-dimensional Brillouin zone showing the high symmetry point along which the band structure was calculated.

We calculate the in-plane stiffness of MX_2 monolayers using the energy-strain relationship as described by Topsakal et al.[40] The in-plane stiffness is defined as:

$$I = \frac{1}{A_0} \frac{\partial^2 E_s}{\partial \varepsilon^2},$$

where A_0 is the equilibrium area of the monolayer, E_s is the difference between the total energy of the strained structure and the total energy of the system at equilibrium; the uniaxial strain is represented by ε. The strain energy data are fitted to the paraboloid

$$E_s = a\varepsilon_x^2 + b\varepsilon_y^2 + c\varepsilon_x\varepsilon_y.$$

The constants a and b are equal due to the honeycomb lattice symmetry. The expressions used to calculate the in-plane stiffness (I) and Poisson's ratio (ν) are the following:

$$I = hC_{11}\left[1 - \left(\frac{C_{11}}{C_{12}}\right)^2\right] = \frac{1}{A_0}\left[2a - \frac{c^2}{2a}\right],$$

$$\nu = \frac{C_{12}}{C_{11}} = \frac{c}{2a},$$

where h is the thickness of the slab.

III. STRUCTURES, STABILITY, AND ELASTIC CONSTANTS

A. Structural relaxation and monolayer stability

The lack of van der Waals interlayer interactions in the MX_2 single layers is expected to cause structural relaxations.[41] The equilibrium lattice parameters, band gap, cohesive energy, stiffness and Poisson's ratio of the various monolayers are summarized in Table I. Consistent with prior studies,[23,29] we observe an expansion of about 1–2% in the in-plane lattice constant a when going from the bulk to a

TABLE I. Basic properties of MX_2 monolayers. a_0 refers to the optimized lattice parameter, E_{gap} is the band gap calculated with the PBE exchange-correlation functional, d and i indicates direct or indirect band gap, respectively. E_f is the formation energy per unit formula of the MX_2 single-layer with respect to the bulk material. I refers to the in-plane stiffness and ν the Poisson's ratio. The in-plane stiffness for single-layer MoS_2 was measured by Bertolazzi et al.[44] to be 180 Nm^{-1}.

2H structures	a_0(Å)	E_{gap} (eV)	E_f (eV/u.f.)	I (N/m)	ν
MoS_2	3.19	1.59(d)	0.18	120.09	0.25
$MoSe_2$	3.33	1.33(d)	0.18	101.48	0.23
$MoTe_2$	3.55	0.93(d)	0.22	72.5	0.25
WS_2	3.19	1.55(d)	0.18	135.18	0.22
WSe_2	3.32	1.27(d)	0.19	112.35	0.20
WTe_2	3.55	0.80(d)	0.25	90.95	0.18
1T structures	a_0(Å)	E_{gap} (eV)	E_f (eV/u.f.)	I (N/m)	ν
HfS_2	3.66	1.26(i)	0.19	74.28	0.19
$HfSe_2$	3.79	0.49(i)	0.19	64.09	0.20
SnS_2	3.71	1.55(i)	0.19	66.04	0.24
$SnSe_2$	3.87	0.73(i)	0.20	55.28	0.24

mono-layer. The separation between the metal and chalcogen layers remains essentially unchanged. We calculated the internal position parameter z in bulk compounds to be ~ 0.121 for M = Mo, W and ~ 0.258 for M = Sn, these are in good agreement with experimental values of 0.129 and 0.240, respectively.[42] Some of these materials have yet to be produced as single layers and in order to quantify whether thermodynamic factors could hinder their fabrication we computed the relative stability with respect to the bulk (total energy difference per formula unit). The energy difference between single-layer and bulk materials range between 0.19 and 0.25 eV per formula unit, see Table I, indicating that the monolayer stability across these systems is similar. The relaxed crystal structure for the transition metal dichalcogenide monolayers is available for online simulation on the Quantum Espresso tool[43] in nanoHUB.org.

B. Elastic constants

Finally, knowing the stiffness of the materials is critical to understand and engineer strain, yet experimental measurements for free standing 2D materials remain challenging.[44] We computed the 2D elastic stiffness of all the monolayers by constructing a grid of 5 by 5 energy-strain points within a uniaxial strain range between -2% and 2%. The resulting values are plotted against lattice parameter in Figure 2. We observe a marked softening with increasing lattice parameter as we move down the chalcogen row for all systems with stiffness ranging from ~ 140 N/m to ~ 50 N/m. These values can be compared with those for graphene obtained from DFT-PBE (335 N/m),[45,46] which is in agreement with the experimental value of 340 ± 40 measure via nanoindentation in an atomic force microscope.[47] We also observe that within the 2H monolayers, the WX_2 systems are consistently stiffer than the MoX_2 monolayers. HfX_2 monolayers exhibit a slightly higher stiffness than the $SnX2$ systems, but the overall stiffness of these systems is low ranging from 55 to 75 N/m.

In order to analyze the implications of the softening with increasing bond distance, let us consider a system with quadratic bonds between nearest neighboring atoms. The energy as a function of strain (ε) can be written (for isotropic deformations) as: $E_s = \frac{Z}{4}K(a\varepsilon)^2$, where Z, K, and a are the coordination number, bond stiffness, and equilibrium bond
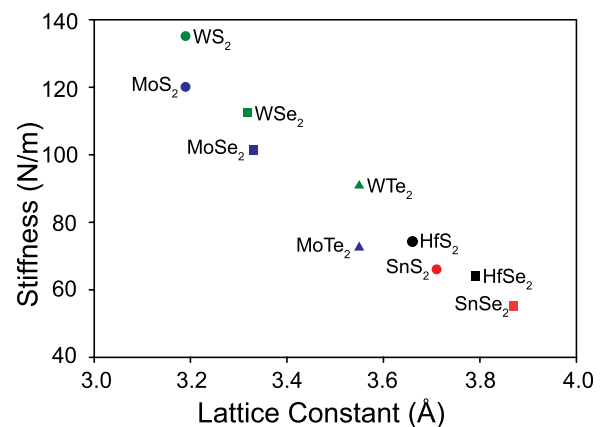

FIG. 2. Calculated 2D stiffness as function of lattice parameter.

distance, respectively. In 3D, the stiffness of such a material scales with a^{-1}. For example, the bulk modulus is $B \sim a^{-3} \left(\frac{\partial^2 E_s}{\partial \varepsilon^2} \right) = \frac{Z}{2a}$. In 2D, we use in-plane stiffness, $\frac{1}{A_0} \frac{\partial^2 E_s}{\partial \varepsilon^2}$, due to the ambiguity in the definition of volume. In this case, the spring model leads to stiffness independent of lattice parameter. Thus, to first order, the predicted softening relates directly to a decrease in bond stiffness.

IV. ELECTRONIC STRUCTURE AND THE ROLE OF STRAIN

A. Band Structure of monolayer transition metal dichalcogenides

The absence of adjacent MX$_2$ layers induces strong modifications to the electronic structure of the monolayer systems due to quantum confinement. For systems consisting of M = Mo, W and X = S, Se, Te, we observed a transition from indirect band gap in the bulk material to direct band gap in the single-layer with the VB maximum and CB minimum centered at the K point of the first Brillouin zone; Figures S2 and S3 in the supplementary material[48] show the electronic band structure of all the MX$_2$ single-layer systems investigated in this work. This observation is consistent with experimental evidence showing the direct band gap character in MoS$_2$ monolayers[19,49,50] and prior calculations.[16,23,29] Although there is no experimental observation of direct band gap in WS$_2$ or WSe$_2$, we expect our results to be accurate based on the ability of *ab initio* methods to successfully describe the electronic structure of other bulk and few-layer transition metal dichalcogenides that have been previously studied experimentally, as is demonstrated for the MoS$_2$ case. On the other hand, our simulations show that monolayers consisting of Sn and Hf atoms do not exhibit a direct band gap, as shown for HfS$_2$ and SnS$_2$, see Figure S3.[48] However, the VB maximum shifts from ~0.5 ΓK in bulk to ~0.3 ΓM in the single-layer, while the CB minimum shifts from L to M.

Band alignment of all unstrained materials is presented in Figure S4 (Ref. [48]). Consistent with recent studies,[21,22,29] we observe that the band edges of 2H MX$_2$ monolayers increase in energy as we move down in the chalcogen row, from S to Te. Overall, the VB maximum and CB minimum of WX$_2$ systems are energetically higher than MoX$_2$ structures.[29] On the other hand, for the SnX$_2$ monolayers, the VB maximum increases in energy when X is changed from S to Se, while the CB minimum remains essentially unchanged at about -5.1 eV (remember these energies are referenced to the vacuum potential). In the case of single-layer HfX$_2$, the energy position of the VB maximum and CB minimum is consistent with the trends observed for (Mo,W)X$_2$ systems. As was recently reported,[22] (Hf, Sn)(S, Se)$_2$ monolayers are good candidates to form type-III heterostructures with Mo(Se, Te)$_2$ and W(Se, Te)$_2$. The main challenge is now determining how strain affects the band alignments of the possible heterostructures.

B. The role of strain

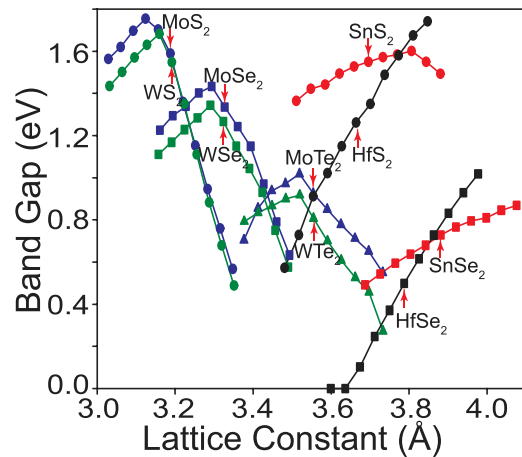To study to role of mechanical deformation, we apply a uniform biaxial strain in the range of -5% to 5% to all

FIG. 3. Band gap as function of the lattice constant for the different MX$_2$ monolayers studied. Each monolayer was strained biaxially in the range of $+/-5\%$. The red arrow indicates the equilibrium lattice constant.

systems. As shown in Figure 2, all the monolayers studied, with the exception of HfSe$_2$, remain semiconductors within the applied strain range. Figure 3 shows that the electronic properties of these materials have a strong and complex dependence on strain. A 1% increase in the lattice parameter of Mo(W)S$_2$ monolayers results in a reduction of the band gap of approximately 0.2 eV while for HfS$_2$ and HfSe$_2$ the same strain increases the band gap by 0.1 eV. The band gap of Sn(S,Se)$_2$ is significantly less sensitive to deformation: approximately 0.02 eV change per 1% strain. As mentioned above, these band gaps come directly from the DFT calculations and the real values are expected to be approximately 50% larger.

In order to discuss band alignment in possible heterostructures, Figure 4 shows the band edge energies with respect to vacuum for selected MX$_2$ monolayers as function of the lattice parameter. The significant sensitivity of the VB maximum and CB minimum energies to slight variations in the lattice parameter suggests significant flexibility in tuning the band edge positions for specific applications but also
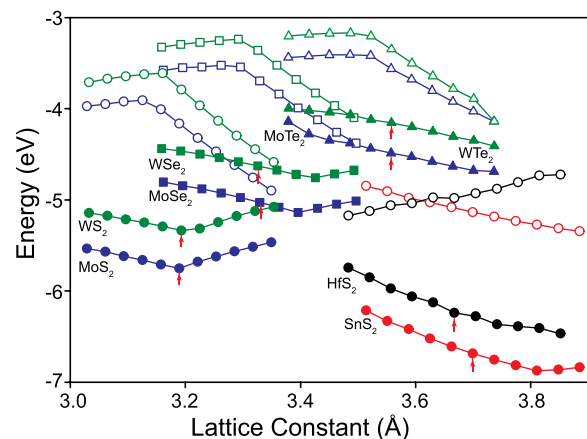

FIG. 4. Absolute VB maximum and CB minimum position for selected cases as function of lattice constant. The vacuum level has been taken as reference and biaxial strain is varied from -5% to 5% in steps of 1% with respect to the equilibrium lattice constant for each system. The red arrows indicate the equilibrium lattice parameter for each material.
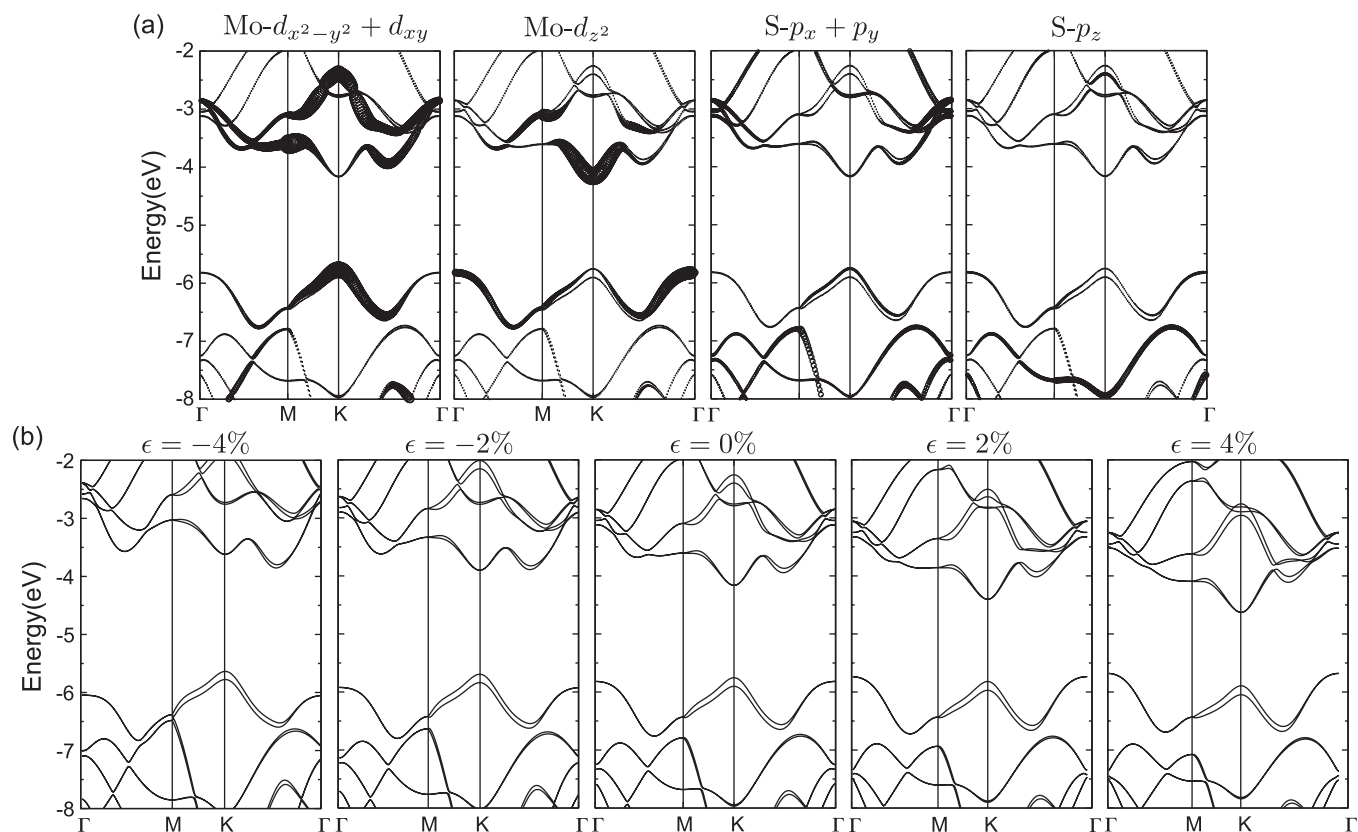
FIG. 5. (a) Computed character band structure of unstrained MoS_2 monolayer. The thickness of the bands is proportional to metallic $d_{x^2-y^2} + d_{xy}$ and d_{z^2} states, and chalcogen $p_x + p_y$ and p_z states. (b) Computed band structure for strained MoS_2 monolayer in the range of -4% to 4%.

point to the fact the small levels of strain can affect device performance.

The 2H sulfide monolayers exhibit a minimum in the VB at their equilibrium lattice parameter (arrows in Figure 4); this minimum move towards larger strains (tension) as we move down the chalcogen row to Se and Te. A maximum in the CB minimum is observed in all 2H monolayers under approximately 2% compression; this maximum marks the transition from direct to indirect character of the band structure. On the other hand, the VB maximum and CB minimum of the 1T monolayers exhibit a monotonic behavior with respect to strain. The difference in behavior of the CB minimum with strain for HfS_2 and SnS_2 are responsible for the significant difference in strain sensitivity of these two materials.

C. Strain effects on band structure

Analysis of the partial density of states and atomic-orbital-resolved band structure of $2H$-MX_2 monolayers provides insight into the origin of the strain effects discussed above. Let us focus first on the 2H structures and their abrupt changes in slope of the VB maxima with tension and that of the CB minima in compression, see Figure 5. These changes in slope are a direct consequence of transitions in the k vector associated the band edges. The VB local maxima at K is dominated by $d_{x^2-y^2} + d_{xy}$ (in-plane) metallic states, while the local maxima at Γ is dominated by metallic d_{z^2} (out-of-plane) states, see Figure 5(a). As the in-plane lattice

parameter is increased (tension), the X-M-X angle is reduced and, consequently, the overlap of metallic d_{z^2} and chalcogen p states is reduced while the coupling of metallic $d_{x^2-y^2} + d_{xy}$ and chalcogen p states is strengthened. The increased overlap of in-plane orbitals with tension can explain the decrease in energy of the VB edge around K (dominated by $d_{x^2-y^2} + d_{xy}$ orbitals) with respect to those around Γ (d_{z^2} orbitals). As a result, tensile strain leads to the band gap becoming indirect with VB maximum and CB minimum centered at Γ and K, respectively.

On the other hand, the CB local minima at K is primarily derived from metallic d_{z^2} states and the local minima along $\Gamma-K$ is dominated by metallic $d_{x^2-y^2} + d_{xy}$ states. Consistent with the explanation above, compressive strain has the effect of shifting the energy levels of the $d_{x^2-y^2} + d_{xy}$ anti-bonding states lower than that of the d_{z^2} anti-bonding states, resulting in an indirect band gap with VB maximum centered at K and CB minimum centered at ΓK. These observations are consistent across all the studied monolayers belonging to the 2H structure, that is, $Mo(S,Se,Te)_2$ and $W(S,Se,Te)_2$.

In the case of the $1T$-MX_2 monolayers, the electronic band structures of SnX_2 and HfX_2 have similar features, however, they differ in the atomic orbital character that give rise to the bonding and anti-bonding bands.

The VB maximum of SnS2 along ΓM is mainly derived from chalcogen $p_x + p_y$ states while the bonding states around ΓK originate from p_z states. Upon tensile strain, the energy levels of the in-plane bonding p states become lower
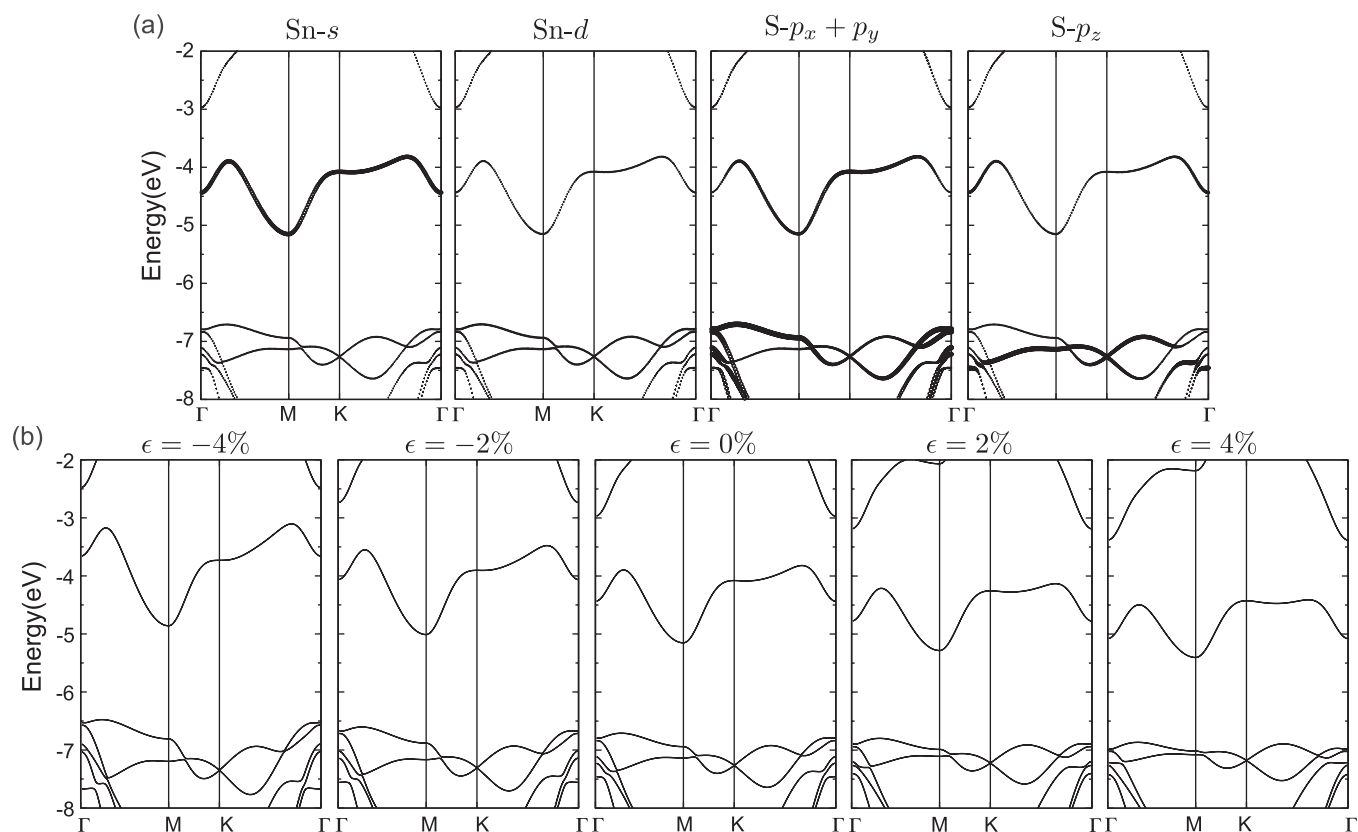
FIG. 6. (a) Computed character band structure of unstrained SnS_2 monolayer. The thickness of the bands is proportional to metallic s and d states, and chalcogen $p_x + p_y$ and p_z states. (b) Computed band structure for strained SnS_2 monolayer in the range of -4% to 4%.

than that of the bonding out-of-plane p states, resulting in a crossover of the VB maximum from ΓM to ΓK, thus the band gap remains indirect but now with CB minimum centered at M and VB maximum centered at ΓK. In compression, the energy levels of the out-of-plane p states are lower than that of the in-plane p states, thus the VB maximum is pinned at ΓM for all the compressive strain states studied. On the other hand, the lower anti-bonding band is derived mainly from Sn's s and chalcogen in-plane p states, as shown in Fig. 6(a). Although the energy of the CB shifts up and down for compressive and tensile strain, respectively, it is observed that the CB minimum does not shift in wave vector. It should be noted that according to the general trend for tensile strain it is expected that the CB minimum will transit from M to Γ for strains greater than 8%.

Similarly, we notice that within the strain states applied, the HfX_2 monolayers conserve an indirect band gap with VB maximum centered at Γ and CB minimum at M. As shown in Figure 7(a), the VB at Γ is mostly derived form chalcogen $p_x + p_y$ states while the VB at ΓK is derived from chalcogen p_z states. Consistent with the trends shown by the VB of SnX_2 monolayers, tensile strain has the effect of lowering the relative energy between the VB maximum at Γ (in-plane p) and ΓK (out-of-plane p). On the other hand, the CB at M is derived from metallic $d_{xz} + d_{yz}$ and d_{z^2} states and its response to strain differs from all the other studied systems. Modulation of the overlap of $d_{xz} + d_{yz}$ and d_{z^2} atomic orbitals caused by strain has the effect of shifting the CB minimum up for tensile and down for compressive strains.

D. Implications for heterostructure design

Recent developments[51] in the fabrication of hybrid MoS_2-graphene[52] and WS_2-graphene[53] vertical heterostructures have raised much interest in the possibility of synthesizing free standing MX_2 heterostructures tailored to a wide variety of applications. In this context, we discuss the possibility of forming type-III heterostructures with the studied MX_2 monolayers. In order to account for the known underestimation of the band gap in the Kohn Sham DFT-PBE band structures the discussion includes the GW-based 50% correction, mentioned above.[32]

The strong dependence of band edge energies on strain provides great flexibility in the design of heterostructures if strain could be independently controlled on the two materials but restricts options in epitaxial heterostructures, i.e., when the two materials share the same lattice parameter. While broken gap heterostructures cannot be formed with unstrained 2H materials, our results show that strain may enable them. For example, our calculations predict that MoS_2 or WS_2 in tension combined with $MoTe_2$ or WTe_2 under compression would form broken gap heterostructures even after the 50% GW correction is applied. This would occur for a lattice parameter of approximately 3.35 Å and would require a significant strain on both materials (about 5%); while large this might be possible at the nanoscale and for 2D materials.[54] Broken gap heterostructures could also be formed between Mo and W tellurides and 1T 2D materials over a larger range of lattice parameters and involving smaller strains.
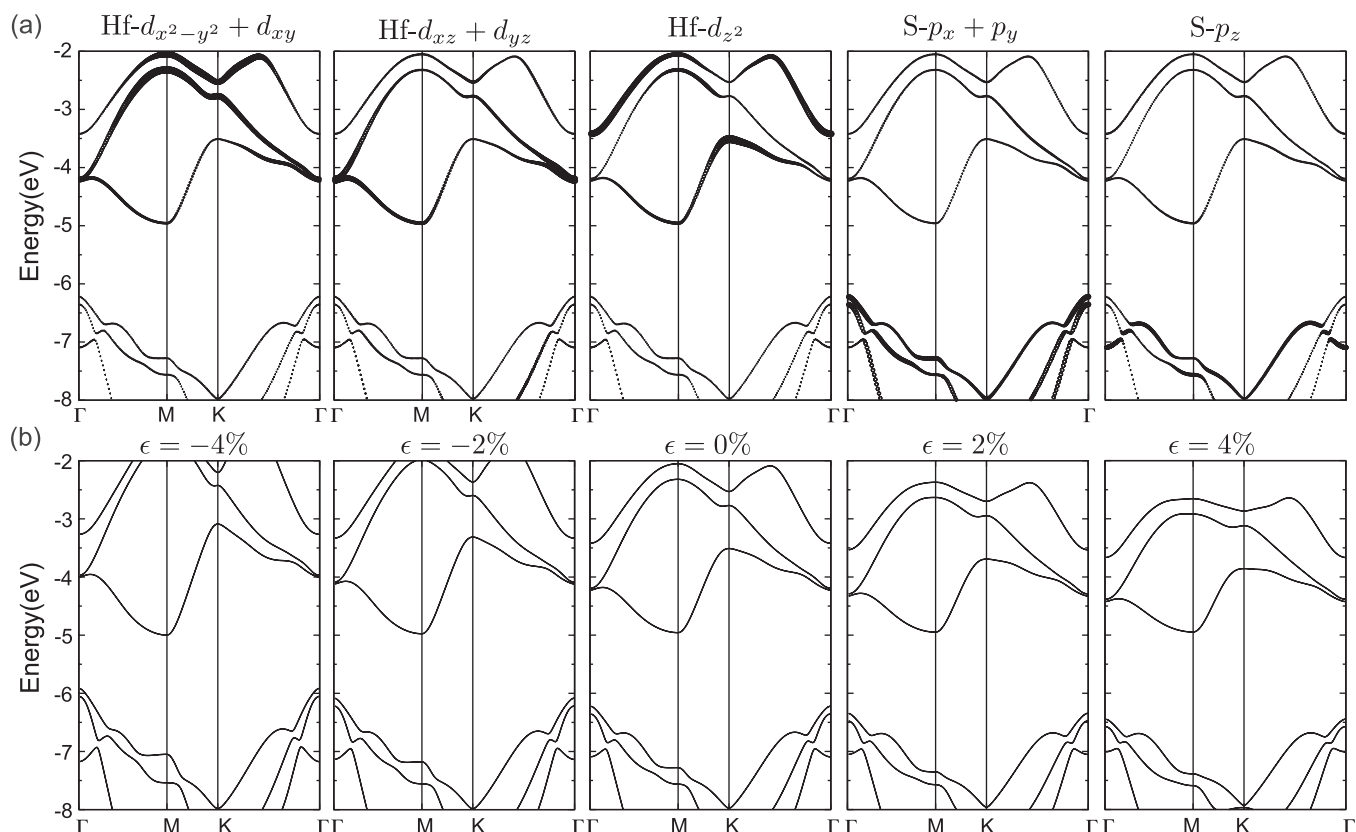
FIG. 7. (a) Computed character band structure of unstrained HfS$_2$ monolayer. The thickness of the bands is proportional to metallic $d_{x^2-y^2} + d_{xy}$, $d_{xz} + d_{yz}$ and d_{z^2} states, and chalcogen $p_x + p_y$ and p_z states. (b) Computed band structure for strained HfS$_2$ monolayer in the range of -4% to 4%.

V. CONCLUSIONS

In summary, we performed a systematic study of the electronic properties of monolayer transition metal dichalcogenides as a function of strain. While some of these 2D materials have not been experimentally realized, their stability indicates no thermodynamic obstacles to their synthesis. The band alignment across the series shows significant flexibility in building heterostructures consisting of single-layers semiconducting materials of interest in a variety of applications. Our predictions indicate several options to create type-III, broken gap, heterostructures and that strain should be carefully considered in such designs.

[1]K. Novoselov *et al.*, "Two-dimensional atomic crystals," Proc. Natl. U.S.A. **102**(30), 10451–10453 (2005).
[2]X. S. Li *et al.*, "Large-area synthesis of high-quality and uniform graphene films on copper foils," Science **324**(5932), 1312–1314 (2009).
[3]Y. J. Zhan *et al.*, "Large-area vapor-phase growth and characterization of MoS$_2$ atomic layers on a SiO2 substrate," Small **8**(7), 966–971 (2012).
[4]X. Huang *et al.*, "Graphene-based materials: synthesis, characterization, properties, and applications," Small **7**(14), 1876–1902 (2011).

[5]Z. P. Yang *et al.*, "Experimental observation of extremely weak optical scattering from an interlocking carbon nanotube array," Appl. Opt. **50**(13), 1850–1855 (2011).
[6]N. R. Pradhan *et al.*, "Intrinsic carrier mobility of multi-layered MoS$_2$ field-effect transistors on SiO$_2$," Appl. Phys. Lett. **102**(12) 123105 (2013).
[7]R. K. Srivastava *et al.*, "Functionalized multilayered graphene platform for urea sensor," ACS Nano **6**(1), 168–175 (2012).
[8]J. J. Yoo *et al.*, "Ultrathin planar graphene supercapacitors," Nano Lett. **11**(4), 1423–1427 (2011).
[9]W. Z. Bao *et al.*, "Controlled ripple texturing of suspended graphene and ultrathin graphite membranes," Nature Nanotechnol. **4**(9), 562–566 (2009).
[10]Z. Zeng *et al.*, "Single-layer semiconducting nanosheets: High-yield preparation and device fabrication," Angew. Chem. Int. Ed. Engl. **50**(47), 11093–11097 (2011).
[11]R. A. Gordon *et al.*, "Structures of exfoliated single layers of WS$_2$, MoS$_2$, and MoSe$_2$ in aqueous suspension," Phys. Rev. B **65**(12) 125407 (2002).
[12]D. Kim *et al.*, "Toward the growth of an aligned single-layer MoS$_2$ film," Langmuir **27**(18), 11650–11653 (2011).
[13]S. Kirmayer *et al.*, "Self-assembled lamellar MoS$_2$, SnS$_2$ and SiO$_2$ semiconducting polymer nanocomposites," Philos. Trans. Roy. Soc. A. Math. Phys. Eng. Sci.. **365**(1855), 1489–1508 (2007).
[14]Y. F. Sun *et al.*, "Freestanding tin disulfide single-layers realizing efficient visible-light water splitting," Angew. Chem.-Int. Ed. **51**(35), 8727–8731 (2012).
[15]C. Ataca, H. Sahin, and S. Ciraci, "Stable, single-layer MX$_2$ transition-metal oxides and dichalcogenides in a honeycomb-like structure," J. Phys. Chem. C **116**(16), 8983–8999 (2012).
[16]Y. Ding *et al.*, "First principles study of structural, vibrational and electronic properties of graphene-like MX$_2$ (M = Mo, Nb, W, Ta; X = S, Se, Te) monolayers," Physica B: Condensed Matter **406**(11), 2254–2260 (2011).
[17]A. Kumar and P. K. Ahluwalia, "Electronic structure of transition metal dichalcogenides monolayers 1H-MX$_2$ (M = Mo, W; X = S, Se, Te) from ab-initio theory: New direct band gap semiconductors," Eur. Phys. J. B **85**(6) 186 (2012).
[18]Y. D. Ma *et al.*, "Electronic and magnetic properties of perfect, vacancy-doped, and nonmetal adsorbed MoSe$_2$, MoTe$_2$ and WS$_2$ monolayers," Phys. Chem. Chem. Phys. **13**(34), 15546–15553 (2011).

[19]K. F. Mak *et al*., "Atomically thin MoS_{2}: A new direct-gap semiconductor," Phys. Rev. Lett. **105**(13), 136805 (2010).

[20]S. Tongay *et al*., "Thermally driven crossover from indirect toward direct bandgap in 2D semiconductors: MoSe$_2$ versus MoS$_2$," Nano Lett. **12**(11), 5576–5580 (2012).

[21]H. L. Zhuang and R. G. Hennig, "Computational search for single-layer transition-metal dichalcogenide photocatalysts," J. Phys. Chem. C **117**(40), 20440–20445 (2013).

[22]C. Gong *et al*., "Band alignment of two-dimensional transition metal dichalcogenides: Application in tunnel field effect transistors," Appl. Phys. Lett. **103**(5), 053513 (2013).

[23]W. S. Yun *et al*., "Thickness and strain effects on electronic structures of transition metal dichalcogenides: 2H-MX_{2} semiconductors (M = Mo, W; X = S, Se, Te)," Phys. Rev. B **85**(3), 033305 (2012).

[24]B. Radisavljevic *et al*., "Single-layer MoS$_2$ transistors," Nature Nanotechnol. **6**(3), 147–150 (2011).

[25]B. Radisavljevic, M. Whitwick, and A. Kis, "Integrated circuits and logic operations based on single-layer MoS$_2$," ACS Nano **5**(12), 9934–9938 (2011).

[26]M. Bernardi, M. Palummo, and J. C. Grossman, "Semiconducting monolayer materials as a tunable platform for excitonic solar cells," ACS Nano **6**(11), 10082–10089 (2012).

[27]M. Shanmugam *et al*., "Molybdenum disulphide/titanium dioxide nanocomposite-poly 3-hexylthiophene bulk heterojunction solar cell," Appl. Phys. Lett. **100**(15), 153901 (2012).

[28]F. K. Perkins, A. L. Friedman, E. Cobas, P. M. Campbell, G. G. Jernigan, and B. T. Jonker, Nano Lett. **13**(2), 668–673 (2013).

[29]J. Kang *et al*., "Band offsets and heterostructures of two-dimensional semiconductors," Appl. Phys. Lett. **102**(1), 012111 (2013).

[30]Z. Y. Zhu, Y. C. Cheng, and U. Schwingenschlögl, "Giant spin-orbit-induced spin splitting in two-dimensional transition-metal dichalcogenide semiconductors," Phys. Rev. B **84**(15), 153402 (2011).

[31]P. Johari and V. Shenoy, "Tuning the electronic properties of semiconducting transition metal dichalcogenides by applying mechanical strains," ACS nano **6**(6), 5449–5456 (2012).

[32]Y. F. Liang *et al*., "Quasiparticle band-edge energy and band offsets of monolayer of molybdenum and tungsten chalcogenides," Appl. Phys. Lett. **103**(4) 042106 (2013).

[33]P. Blaha *et al*., *WIEN2k*, "An Augmented Plane Wave + Local Orbitals Program for Calculating Crystal Properties" (Karlheinz Schwarz, Techn. Universität Wien, Austria, 2001).

[34]J. P. Perdew, K. Burke, and M. Ernzerhof, "Generalized gradient approximation made simple," Phys. Rev. Lett. **77**(18), 3865–3868 (1996).

[35]A. H. Macdonald, W. E. Pickett, and D. D. Koelling, "A linearized relativistic augmented-plane-wave method utilizing approximate pure spin basis functions," J. Phys. C-Solid State Phys. **13**(14), 2675–2683 (1980).

[36]M. C. Toroker *et al*., "First principles scheme to evaluate band edge positions in potential transition metal oxide photocatalysts and photoelectrodes," Phys. Chem. Chem. Phys. **13**(37), 16644–16654 (2011).

[37]P. Giannozzi *et al*., "QUANTUM ESPRESSO: A modular and open-source software project for quantum simulations of materials," J. Phys.-Condens. Matter **21**(39), 19 (2009).

[38]P. E., Blochl, "Projector augmented-wave method," Phys. Rev. B **50**(24), 17953–17979 (1994).

[39]H. J. Monkhorst and J. D. Pack, "Special points for brillouin-zone integrations," Phys. Rev. B **13**(12), 5188–5192 (1976).

[40]M. Topsakal, S. Cahangirov, and S. Ciraci, "The response of mechanical and electronic properties of graphane to the elastic strain," Appl. Phys. Lett. **96**(9) 091912 (2010).

[41]C. Lee *et al*., "Anomalous lattice vibrations of single- and few-layer MoS$_2$," ACS Nano **4**(5), 2695–2700 (2010).

[42]R. Coehoorn *et al*., "Electronic-structure of MoSe$_2$, MoS$_2$, and Wse2.1. Band-structure calculations and photoelectron-spectroscopy," Phys. Rev. B **35**(12), 6195–6202 (1987).

[43]J. Jhaveri *et al*., see https://nanohub.org/resources/dftqe for DFT calculations with Quantum ESPRESSO, 2010.

[44]S. Bertolazzi, J. Brivio, and A. Kis, "Stretching and breaking of ultrathin MoS$_2$," Acs Nano **5**(12), 9703–9709 (2011).

[45]M. Topsakal and S. Ciraci, "Elastic and plastic deformation of graphene, silicene, and boron nitride honeycomb nanoribbons under uniaxial tension: A first-principles density-functional theory study," Phys. Rev. B **81**(2), 024107 (2010).

[46]R. Faccio *et al*., "Mechanical properties of graphene nanoribbons," J. Phys.-Condens. Matter **21**(28), 285304 (2009).

[47]C. Lee *et al*., "Measurement of the elastic properties and intrinsic strength of monolayer graphene," Science **321**(5887), 385–388 (2008).

[48]See supplementary material at http://dx.doi.org/10.1063/1.4883995 for the complete electronic structure of the studied MX2 monolayers.

[49]T. S. Li and G. L. Galli, "Electronic properties of MoS$_2$ nanoparticles," J. Phys. Chem. C **111**(44), 16192–16196 (2007).

[50]A. Splendiani *et al*., "Emerging photoluminescence in monolayer MoS$_2$," Nano Lett. **10**(4), 1271–1275 (2010).

[51]J. N. Coleman *et al*., "Two-dimensional nanosheets produced by liquid exfoliation of layered materials," Science **331**(6017), 568–571 (2011).

[52]S. Bertolazzi, D. Krasnozhon, and A. Kis, "Nonvolatile memory cells based on MoS$_2$/graphene heterostructures," Acs Nano **7**(4), 3246–3252 (2013).

[53]T. Georgiou *et al*., "Vertical field-effect transistor based on graphene-WS$_2$ heterostructures for flexible and transparent electronics," Nature Nanotechnol. **8**(2), 100–103 (2013).

[54]A. Arumbakkam, E. Davidson, and A. Strachan, "Heteroepitaxial integration of metallic nanowires: Transition from coherent to defective interfaces via molecular dynamics," Nanotechnology **18**(34) 345705 (2007).